IL NUOVO CIMENTO Vol. 26 C, N. 3 Maggio-Giugno 2003

The parameterization of microphysical processes for atmospherical numerical models

O. V. Drofa
CNR, ISAC - Via P. Gobetti 101, I-40129 Bologna, Italy

(ricevuto l'1 Luglio 2002; revisionato il 10 Marzo 2003; approvato l'11 Aprile 2003)

Summary. — This paper presents a parametrization of microphysical cloud and precipitation processes set up for application in atmospheric numerical models. The parametrization includes the approximation of processes regarding the formation and the evolution of atmospheric condensate in both the liquid and solid phase. The algorithm is based on the entropy conservation law for a closed thermodynamic system that includes water vapour, cloud water, cloud ice, liquid and solid hydrometeors. Some original methods of cloud evolution approximation are used in the scheme; in particular a more accurate method of parametrization of hydrometeor evaporation and sublimation is applied. The presented parametrization is tested in two different atmospheric numerical models. The first model is a two-dimensional, non-hydrostatic cumulonimbus model; and the second one is the mesoscale hydrostatic model BOLAM. With the cumulonimbus model the parametrization verification is performed on the basis of the observations; the comparison with other microphysical schemes is also made. The analysis of the cumulonimbus life cycle, and the role played by microphysical processes in cloud and precipitation evolution, is presented. With the BOLAM model, the comparison between the present microphysical scheme and the one based on a more simplified microphysical parameterization is performed.

PACS 92.60.Wc – Weather analysis and prediction.
PACS 92.60.Jq – Water in the atmosphere (humidity, clouds, evaporation, precipitation).

1. – Introduction

During recent years, the development of higher-resolution atmospheric models has imposed the need for accurate parametrizations of microphysical processes. Microphysical parametrizations are usually based on the results of numerous theoretical and observational studies. These studies show which physical processes are more important for the formation of clouds and precipitation. The first microphysical parametrization, which was developed for numerical modelling purposes by Kessler [1], omitted the ice phase of atmospheric water. In spite of this strong approximation, the work of Kessler constituted

a basis for more modern and sophisticated parametrizations. Among the best known are the ones of Lin *et al.* [2] and Rutledge and Hobbs [3]. The most general results of theoretical and empirical research are used in these parametrizations, which are employed in many high-resolution weather prediction models. The parametrizations differ mainly in the way in which they apply the most recent empirical results, which provide new data on clouds and precipitation microcharacteristics, and on the relative contributions of various microphysical processes. One example of such studies is the parametrization of Marecal *et al.* [4].

In this work, a new microphysical parametrization for numerical models of the atmosphere (mesoscale research and operational models) is presented. This parametrisation is designed on the basis of the contemporary ideas and results concerning microphysics, with some approximations done keeping in mind the practical applicability, both in terms of simplicity of coding and of computational load, to an operational weather prediction model. It uses the entropy conservation law, which was originally proposed by Pressman (in [5, 6]) as a very suitable method for representing water phase transitions for atmospheric models. The principle of the scheme proposed here lies in the separation of the microphysical processes into two principal groups: the group of "fast" (almost instantaneous) processes and the group of "slow" processes. The first group contains the mutual interaction between water vapour, cloud water, and cloud ice, while the second group describes the formation/depletion of liquid and solid precipitation as a function of the specific concentration of water vapour, cloud water, cloud ice, and precipitations themselves. Here, solid precipitation is represented by one type of hydrometeors only, but its aerodynamic characteristics and density vary as a function of temperature in order to partly take into account the different types of hydrometeors prevailing at different temperature ranges, like snow flakes, graupel, hail. The parametrization of the processes of the second group is based on the principles described in [4,3], where some new features that regard evaporation/deposition processes are introduced.

The paper is organised as follows. In sect. **2**, the description of the physical problem of the proposed parametrization is presented. Sections **3** and **4** include the description of fast and slow processes parametrization, respectively. In sect. **5**, the scheme is tested in the two-dimensional cumulonimbus model of Drofa [7] by performing several case studies in which the vertical profiles of humidity and temperature are specified from observations. This section also presents a sensitivity study aimed at understanding the relative importance of the various microphysical processes. In sect. **6**, the results obtained by introducing the proposed scheme into the mesoscale BOLAM model are compared to those obtained with a scheme based mainly on the simpler parametrization described in [8]. Finally, sect. **7** contains some conclusions.

2. – Physical problem of the microphysical parametrization: equations and hypotheses

The microphysical parametrization proposed here treats 6 components of the atmospheric environment: dry air, water vapour, cloud water, cloud ice, rain and snow. Their evolution processes are separated into two groups: "fast" processes and "slow" processes. The group of fast processes includes the interaction between vapour, cloud ice and cloud water and conserves the total mass of these components. Such processes are considered as instantaneous, *i.e.* with unlimited rate. It is a strong approximation, however, these physical processes have very short time scale, from thousandth to tenth fractions of one second [9], that can be considered instantaneous with respect to the actual time res-

olution of atmospheric numerical models. Such approximation allows us to avoid any hypothesis about rates of fast processes, *i.e.* to avoid the application of a whole series of empirical parameters. At the same time, fast processes description requires the solution of a thermodynamical problem that has some difficult points, and the discussion about that problem will be made below. The second group, that is called slow processes group, includes all processes in which precipitation particles participate, and these processes have their limited time rates provided by their parametrization.

The parametrization uses the description of thermodynamical processes that is based on an original method, proposed in the works of Pressman [5, 6]. In these works it is demonstrated that the application of the entropy conservation equation is a theoretically well founded and very suitable method for the description of thermodynamical processes in an atmospherical model. Here some important principles of that approach will be presented. It must be pointed out that in the present work entropy does not need to be a prognostic variable of the model equation system, and in that case it can be computed at the beginning of the microphysical parametrization.

Entropy is a thermodynamic feature of the atmospheric gaseous system which is formed by the sum of the entropies of the single components:

$$S = q_{\mathrm{d}} s_{\mathrm{d}} + q_{\mathrm{v}} s_{\mathrm{v}} + (q_{\mathrm{cw}} + q_{\mathrm{R}}) s_{\mathrm{w}} + (q_{\mathrm{ci}} + q_{\mathrm{S}}) s_{\mathrm{i}}, \tag{1}$$

where s is the specific entropy, q the specific mass, and where the indices have the following meaning: "d" indicates dry air, "v" water vapour, "cw" and "ci" cloud water and cloud ice, respectively, "R" rain, "S" snow, "w" water, and "i" ice. The specific entropy terms have been determined by Pressman [5]:

$$s_{\mathrm{d}} = C_p^{\mathrm{d}} \ln \frac{T}{T_0} - R_{\mathrm{d}} \ln \frac{p_{\mathrm{d}}}{p_0}, \qquad T_0 = 273.15\,\mathrm{K}, \qquad p_0 = 1000\,\mathrm{hPa}, \tag{2}$$

$$s_{\mathrm{v}} = C_p^{\mathrm{v}} \ln \frac{T}{T_0} - R_{\mathrm{v}} \ln \frac{e}{E_0} + \frac{L_{\mathrm{i}}^{\mathrm{v}}}{T_0}, \qquad E_0 = E_{\mathrm{s}}(T_0, p_0), \tag{3}$$

$$s_{\mathrm{w}} = C_{\mathrm{w}} \ln \frac{T}{T_0} + \frac{L_{\mathrm{i}}^{\mathrm{w}}}{T_0}, \tag{4}$$

$$s_{\mathrm{i}} = C_{\mathrm{i}} \ln \frac{T}{T_0}, \tag{5}$$

where C_p^{d} and C_p^{v} are the specific heat of dry air and water vapour at constant pressure, C_{w} and C_{i} are the specific heat of water and ice, R_{d} and R_{v} are the gas constants of dry air and water vapour, p_{d} and e are the partial pressures of dry air and water vapour, E_{s} is the saturated water vapour pressure, T is the temperature, $L_{\mathrm{i}}^{\mathrm{v}}$ and $L_{\mathrm{i}}^{\mathrm{w}}$ are the latent heat of water sublimation and ice melting, respectively (all constants are listed in appendix A).

Entropy conservation will be used as the basic thermodynamic equation of the present microphysical parametrization, which is thus based on the following system:

$$\frac{\mathrm{d}S}{\mathrm{d}t} = 0, \tag{6}$$

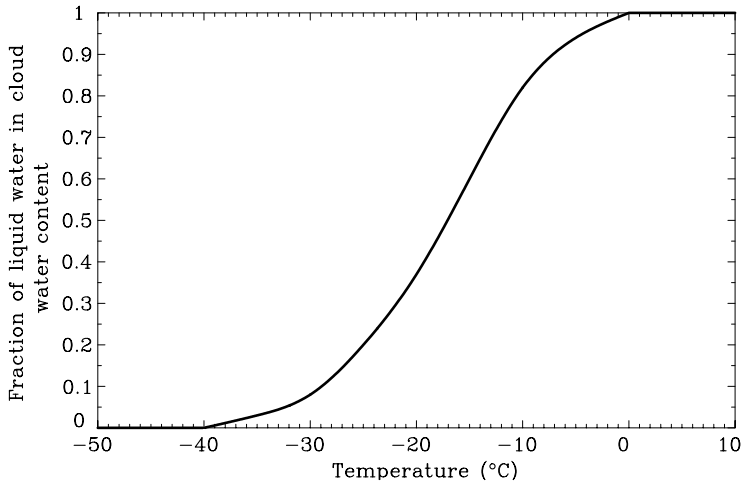

Fig. 1. – The fraction of liquid water in mixed cloud condensate as a function of temperature.

$$\frac{\mathrm{d}q}{\mathrm{d}t} = -M_{\mathrm{R}}^{\mathrm{v,c}} - M_{\mathrm{S}}^{\mathrm{v,c}}, \tag{7}$$

$$\frac{\mathrm{d}q_{\mathrm{R}}}{\mathrm{d}t} = M_{\mathrm{R}}^{\mathrm{v,c}}, \tag{8}$$

$$\frac{\mathrm{d}q_{\mathrm{S}}}{\mathrm{d}t} = M_{\mathrm{S}}^{\mathrm{v,c}}, \tag{9}$$

where $M_{\mathrm{R}}^{\mathrm{v,c}}$ and $M_{\mathrm{S}}^{\mathrm{v,c}}$ are sources and sinks of rain and snow due to the slow microphysical processes and where $q = q_{\mathrm{v}} + q_{\mathrm{cw}} + q_{\mathrm{ci}}$.

Equations (6)-(9) include 6 unknowns, so they must be completed by 2 more equations in order to form a closed system. These equations arise from the relationship giving the saturated vapour pressure. From the Clausius-Clapeyron equation and the expression of the specific entropy, the equation of saturated vapour pressure can be written as in [6]:

$$E_{\mathrm{sk}} = E_0 \exp\left[\frac{C_p^{\mathrm{v}} - C_{\mathrm{k}}}{R_{\mathrm{v}}} \ln\frac{T}{T_0} + \left(\frac{L_{\mathrm{k}}^{\mathrm{v}}}{T_0 R_{\mathrm{v}}} - \frac{C_p^{\mathrm{v}} - C_{\mathrm{k}}}{R_{\mathrm{v}}}\right)\left(1 - \ln\frac{T}{T_0}\right)\right], \tag{10}$$

where the index k can be either w or i and indicates the substance over which vapour is saturated: water or ice. Equation (10) is in agreement with the entropy conservation but, in principle, other expressions can be used in a microphysical parametrization to determine saturated vapour pressure as function of temperature.

The proposed scheme includes the existence of a mixed (solid and liquid) water condensate at temperatures below 0 °C. It means that in eq. (7) each of the variables q_{v}, q_{cw}, q_{ci} can be nonzero at a particular temperature range, so it must be possible to compute each of them from their sum (q). In this situation the equations for specific mass of vapour saturated over water and ice are not sufficient, and for resolution of eq. (7) two additional hypotheses must be assumed.

Therefore, it is proposed to fix the relation between liquid and solid cloud condensates as a function of temperature only. This relation can actually depend on the type of the

cloud, on its origin and evolution, however, according to aircraft observations, the large majority of its variations is determined by temperature. In the handbook [9] the results of a statistical analysis of dependence of cloud phase on temperature, based on a huge number of aircraft observations, is presented. The results of this analysis are used here for determining the fraction of liquid water in the mixed cloud, and the function used is shown in fig. 1:

$$F(T) = \frac{q_{\mathrm{cw}}}{q_{\mathrm{cw}} + q_{\mathrm{ci}}}. \tag{11}$$

The second hypothesis is made in terms of saturated vapour pressure above mixed condensate. Within the limits of thermodynamic equilibrium theory, there is no theoretical evidence of which is the preferable choice for the form of saturated vapour pressure above a water-ice mixture, so a simple and straightforward assumption is to use a linear combination of saturated vapour pressure using the liquid and solid fraction as weights [6]. The equation thus reads

$$E_{\mathrm{mix}}(T) = F(T)E_{\mathrm{sw}}(T) + (1 - F(T))\, E_{\mathrm{si}}(T), \tag{12}$$

where for $F(T)$ the expression (11) is used.

Returning to the discussion about fast processes parametrization, it must be noted that this parametrization includes the problem of the separation of components of the variable q using the approximation that the system approaches the thermodynamic equilibrium described by eqs. (10) and (12) with unlimited rate. Therefore, the fast processes parametrization is based on a diagnostic procedure.

A system of equations for the parametrization is now formulated. For its resolution $M_{\mathrm{R}}^{\mathrm{v,c}}$ and $M_{\mathrm{S}}^{\mathrm{v,c}}$ must be determined, which are related to the "slow microphysical process" parametrization, and a diagnostic procedure must be also set up for determining such variables as temperature, specific cloud water and specific cloud ice; the procedure is referred to as "fast microphysical process" parametrization.

3. – Fast microphysical process parametrization

The basic system (6)-(9) will be solved with respect to the following variables: S, q, q_{R} and q_{S}, which are the prognostic variables. However, the parametrization needs other variables, namely T, q_{v}, q_{cw} and q_{ci}, which are the diagnostic ones. The search for those variables is performed by an approximation of fast microphysical processes, which is based on the idea of the thermodynamic equilibrium and is organised as a diagnostic procedure set up with the following equation system:

$$q = q_{\mathrm{v}} + q_{\mathrm{cw}} + q_{\mathrm{ci}}, \tag{13}$$

$$q_{\mathrm{v}} = F(T)q_{\mathrm{sw}}(T) + [1 - F(T)]q_{\mathrm{si}}(T), \tag{14}$$

$$q_{\mathrm{cw}} = F(T)\,(q - q_{\mathrm{v}})\,, \tag{15}$$

$$\begin{aligned} S = (1 - q - q_{\mathrm{R}} - q_{\mathrm{S}}) \left(C_p^{\mathrm{d}} \ln \frac{T}{T_0} - R_{\mathrm{d}} \ln \frac{p_{\mathrm{d}}}{p_0} \right) + \\ + F(T)q_{\mathrm{v}} \left(C_p^{\mathrm{v}} \ln \frac{T}{T_0} - R_{\mathrm{v}} \ln \frac{E_{\mathrm{sw}}(T)}{E_0} + \frac{L_{\mathrm{i}}^{\mathrm{v}}}{T_0} \right) + \end{aligned} \tag{16}$$

$$+(1-F(T))q_{\mathrm{v}}\left(C_p^{\mathrm{v}}\ln\frac{T}{T_0}-R_{\mathrm{v}}\ln\frac{E_{\mathrm{si}}(T)}{E_0}+\frac{L_{\mathrm{i}}^{\mathrm{v}}}{T_0}\right)+$$
$$+(q_{\mathrm{cw}}+q_{\mathrm{R}})\left(C_{\mathrm{w}}\ln\frac{T}{T_0}+\frac{L_{\mathrm{i}}^{\mathrm{w}}}{T_0}\right)+(q_{\mathrm{ci}}+q_{\mathrm{S}})\left(C_{\mathrm{w}}\ln\frac{T}{T_0}\right);$$

here p_{d} is the (partial) pressure of dry air, $p_{\mathrm{d}}=p-e$, p the atmospheric pressure, and e the water vapour pressure, $e=E_{\mathrm{mix}}$. The system (13)-(16) is written for the case of water vapour saturation, which is the most general case in this study, while the case without saturation (*i.e.* in the absence of clouds) is a particular case, where eqs. (13)-(16) have a simpler form. The system (13)-(16) is closed by eqs. (10) and by the definition of the $F(T)$ function, since they include the following unknown quantities: T, q_{v}, q_{cw}, q_{ci}, $q_{\mathrm{sw}}(T)$ ($E_{\mathrm{sw}}(T)$), $q_{\mathrm{si}}(T)$ ($E_{\mathrm{si}}(T)$) and $F(T)$.

It is possible to solve the system of eqs. (13)-(16) by an iterative procedure, and for this purpose the Newton approximation method is applied. The procedure is organised in the following way: at the beginning of the solution of the system a value for the temperature (T^*) is taken, for example, the value from the previous time-step, T^* is used in the equations of the system to compute $S(T^*)$ using the known values of q, q_{R} and q_{S}. But $S(T^*)\neq S$, and the value of T so that $|S(T)-S|<\varepsilon$ (ε is the desired precision) must be found. The correction of the temperature value for the next iteration is given by the Taylor series approximation up to the first-order term:

$$S^{\Delta t}=S(T^*)+\Delta T^*\frac{\mathrm{d}S(T^*)}{\mathrm{d}T^*}\quad\Rightarrow\quad\Delta T^*=\frac{S^{\Delta t}-S(T^*)}{\frac{\mathrm{d}S(T^*)}{\mathrm{d}T^*}},\tag{17}$$

where $\mathrm{d}S(T^*)/\mathrm{d}T^*$ can be expressed by the analytical formula, but can also be computed numerically with a simpler expression. In this work the more accurate analytical expression is used.

When T is found, q_{v}, q_{cw} and q_{ci} can be determined by eqs. (13), (14), (15).

4. – Slow microphysical process parametrization

The present scheme is based on the ideas of the parametrizations proposed in [4, 3] with the application of new quantitative parameters and a more accurate approximation of evaporation/sublimation of hydrometeors. In the parametrization presented in this work, it is supposed that the precipitation particles have the distribution of Marshall-Palmer [10]:

$$N(D)=N_0e^{-\lambda D},\tag{18}$$

where N is the particle concentration, N_0 and λ are distribution parameters. N_0 is a constant depending on the type of particle forming the precipitation, λ a function of precipitation specific mass (q_{P}, P = R for rain, P = S for snow) and D is the particle diameter. Conversely, for cloud (liquid and solid) particles, there is no hypothesis about their size distribution.

Microprocesses parametrization needs some hypotheses on the relation between particle diameter, mass and terminal falling velocity. Here, the relations of Mason [11] and Langleben [12] are used:

$$m=aD^b,\tag{19}$$

TABLE I. – *The values of the constant coefficients: N_0 is the parameter of the Marshall-Palmer distribution, a, b, k, n are coefficients in eqs. (19) and (20).*

Hydrometeor type	N_0 (m^{-4})	Source of N_0 value	a ($\mathrm{kg\ m}^{-b}$)	b	k ($\mathrm{m}^{1-n}\mathrm{s}^{-1}$)	n	Source of a, b, k, n values
Rain (liquid hydrometeors)	8×10^6	[10]	1000	3	842	0.8	[14]
Snow (solid hydrometeors) I	8×10^6	[3]	232	3.06	144	0.66	[13]
II	2×10^7	[3]	157	3.31	156	0.86	[13]
III	4×10^7	Applied in this work	1.43	2.79	18	0.62	[13]
IV	5×10^7	Applied in this work	0.145	2.59	7.3	0.55	[13]

$$V_\mathrm{t} = kD^n, \tag{20}$$

where m is the particle mass, V_t terminal falling velocity, and a, b, k, n constant values.

In this parametrization all hydrometeor particles are divided into two groups: liquid hydrometeors ("rain") and solid hydrometeors ("snow"). Solid precipitation is not divided into snow and hail. This rough approximation is made firstly for simplifying the parametrization and, secondly, because the microphysical parametrization does not allow to correctly separate solid precipitation into snow and hail, since such separation requires to take into account not only microphysical processes, but also the thermodynamic evolution of a cloud, *i.e.* parameters like temperature and vertical velocity. Since such analysis is unsuitable to the current accuracy of mesoscale models, an explicit description of hail is not made. However, some implicit account of the presence of solid hydrometeor particles having the properties of hail is made here, since, while all rain particles are supposed to have the same aerodynamic features, snow particles have some features that depend on temperature. This dependence allows to consider, to a certain extent, the variety of solid hydrometeors. The variable features, for solid precipitation, are N_0, a, b, k, n that are used in (18), (19), (20). In this work a new study about these variable parameters is done. In nature, the form and, as consequence, the aerodynamic properties of crystal hydrometeors, are determined by thermodynamic conditions of formation and growth of crystals, and a dominant role, among these conditions, is played by temperature. Therefore, at a certain temperature interval, ice particles of a certain form dominate. In the present work the temperature scale is divided into four intervals and for each interval the most representative type of solid particle is determined (the types of precipitation particles are taken from the Magono and Lee classification). The following particles types are chosen: I) conelike graupel (R4c) at $T \geqslant -10\,^\circ\mathrm{C}$, II) hexagonal plate (P1a) at $-10\,^\circ\mathrm{C} > T \geqslant -20\,^\circ\mathrm{C}$, III) crystal with broad branches (P1c) at $-20\,^\circ\mathrm{C} > T \geqslant -30\,^\circ\mathrm{C}$, and IV) stellar crystal (P1d) at $T < -30\,^\circ\mathrm{C}$. For a, b, k, n the values from the study of Heymsfield and Kajikawa [13] are used for the first time. The parameters values for the chosen particles types are presented in table I.

The dependence of the distribution parameter λ upon q_P is obtained as the integral

of particle specific mass, computed with eq. (19), over the whole size spectrum:

$$\lambda_{\mathrm{P}} = \left[\frac{N_{0\mathrm{P}} a_{\mathrm{P}} \Gamma(b_{\mathrm{P}}+1)}{\rho_{\mathrm{a}} q_{\mathrm{P}}}\right]^{1/(b_{\mathrm{P}}+1)}, \tag{21}$$

where Γ is the gamma-function and ρ_{a} is humid air density. It is assumed that rain and snow spectrums of particles fall at their respective mass-weighted mean terminal velocity:

$$U_{\mathrm{tP}} = \frac{\int\limits_0^\infty N_{\mathrm{P}}(D_{\mathrm{P}}) m_{\mathrm{P}}(D_{\mathrm{P}}) V_{\mathrm{tP}}(D_{\mathrm{P}}) \mathrm{d}D_{\mathrm{P}}}{\int\limits_0^\infty N_{\mathrm{P}}(D_{\mathrm{P}}) m_{\mathrm{P}}(D_{\mathrm{P}}) \mathrm{d}D_{\mathrm{P}}}, \tag{22}$$

where for $V_{\mathrm{tP}}(D_{\mathrm{P}})$ eq. (20) is used with an atmospheric pressure dependence correction proposed in Foot and Du Toit [15]: $V_{\mathrm{tP}}(D_{\mathrm{P}}) = k_{\mathrm{P}} D_{\mathrm{P}}^{n_{\mathrm{P}}} \left(\frac{p_0}{p}\right)^{0.4}$, where p is the atmospheric pressure and $p_0 = 1000\,\mathrm{hPa}$.

With all the described hypotheses the following microphysical processes are approximated.

i) Autoconversion of cloud water into rain (RAUT)

This process is parameterised following [1]

$$\mathrm{RAUT} = \alpha_{\mathrm{autw}}(q_{\mathrm{cw}} - q_{\mathrm{cw}}^{\mathrm{th}}), \tag{23}$$

where α_{autw} is the rate coefficient, $q_{\mathrm{cw}}^{\mathrm{th}}$ is a threshold value of q_{cw}, from which the process begins, $\alpha_{\mathrm{autw}} = 10^{-3}\,\mathrm{s}^{-1}$, $q_{\mathrm{cw}}^{\mathrm{th}} = 5 \times 10^{-4}\,\mathrm{kgkg}^{-1}$, this last value is chosen on the basis of numerical experiments.

ii) Autoconversion of cloud ice into snow (SAUT)

This process is parametrised as the previous one, but the rate coefficient depends on the temperature because of the changes in crystal density and aerodynamical features with temperature. For this dependence we applied the formula of Lin *et al.* [2]:

$$\mathrm{SAUT} = \alpha_{\mathrm{auti}} e^{[0.025(T-T_0)]}(q_{\mathrm{ci}} - q_{\mathrm{ci}}^{\mathrm{th}}), \tag{24}$$

α_{auti} is the rate coefficient equal to $10^{-3}\,\mathrm{s}^{-1}$ and $q_{\mathrm{ci}}^{\mathrm{th}}$ is a threshold value of q_{ci}, $q_{\mathrm{ci}}^{\mathrm{th}} = 10^{-3}\,\mathrm{kgkg}^{-1}$.

iii) Evaporation of rain (REVP)

The process of evaporation of precipitation liquid particles is approximated by the diffusion flux theory [11, 16]. Diffusion flux of water vapour transfers water mass from the particle surface to the environmental air; particle mass change rate is

$$\frac{\mathrm{d}m_{\mathrm{EVP}}}{\mathrm{d}t} = 4\pi r \chi F_{\mathrm{v}}(\rho_{\mathrm{v}\infty} - \rho_{\mathrm{vP}}), \tag{25}$$

where r is the particle radius, χ the coefficient of molecular diffusion of vapour into air, F_{v} the vapour ventilation coefficient, $\rho_{\mathrm{v}\infty}$ the vapour density in the environmental air and ρ_{vP} the vapour density on the particle surface.

When this process is in a stationary condition, the heat absorption rate by evaporation is equal to the heat flux rate at the particle surface:

$$L_{\mathrm{w}}^{\mathrm{v}} \frac{\mathrm{d}m_{\mathrm{EVP}}}{\mathrm{d}t} = 4\pi r K_{\mathrm{a}} F_{\mathrm{h}} (T_\infty - T_{\mathrm{P}}), \tag{26}$$

where T_∞ and T_{P} are the temperature of environmental air and of the particle surface, K_{a} is the thermal conductivity, and F_{h} the thermal ventilation coefficient.

Using the definition: $s \equiv \rho/\rho_{\mathrm{s}}$, $\rho = s\rho_{\mathrm{s}}$, where ρ_{s} is vapour saturation density, it follows that

$$\rho_{\mathrm{vP}} = \rho_{\mathrm{s}}(T_{\mathrm{P}}) s_{\mathrm{p}}\,, \tag{27}$$

$$\rho_{\mathrm{v}\infty} = \rho_{\mathrm{s}}(T_\infty) s_\infty\,. \tag{28}$$

Equations (25)-(28) compose the system that can be numerically solved only with an expensive iterative procedure. Therefore, in microphysical parametrizations, an approximation of ρ_{vP} is usually employed. The approximation that is commonly used in microphysical schemes has been proposed by Byers [17] and consists of a Taylor series expansion up to the first order:

$$\rho_{\mathrm{s}}(T_{\mathrm{P}}) \approx \rho_{\mathrm{s}}(T_\infty) + \rho_{\mathrm{s}}'(T_\infty)\Delta T_\infty\,, \qquad \rho_{\mathrm{s}}'(T_\infty) = \left.\frac{\partial \rho}{\partial T}\right|_\infty\,. \tag{29}$$

However, in the work of Srivastava and Coen [18] it is proved that the Byers approximation is not satisfactory when the process of evaporation (condensation) is very rapid. This situation arises, for example, when hydrometeors enter a warm and dry air mass below a cumulonimbus. Thus these authors suggested to extend the Taylor series expansion up to the second order for the approximating mode:

$$\rho_{\mathrm{s}}(T_{\mathrm{P}}) \approx \rho_{\mathrm{s}}(T_\infty) + \rho_{\mathrm{s}}'(T_\infty)\Delta T_\infty + \frac{1}{2}\rho_{\mathrm{s}}''(T_\infty)\Delta T_\infty^2\,. \tag{30}$$

The present work adopts for the first time the more accurate approximation (30) to study the improvement achieved by this method. To obtain the rate of change in particle mass by evaporation (condensation), eqs. (25), (26) (with $T_{\mathrm{P}} - T_\infty = \Delta T_\infty$), (27), (28) and (30) are used supposing that $F_{\mathrm{v}} = F_{\mathrm{h}}$ (the ventilation of heat and vapour are equal) and $s_{\mathrm{P}} = 1$ (saturation condition on the particle surface):

$$\begin{aligned}\frac{\mathrm{d}m_{\mathrm{EVP}}}{\mathrm{d}t} = {} & \frac{2\pi D F \left(\frac{q_{\mathrm{v}}}{q_{\mathrm{sw}}} - 1\right)\rho_{\mathrm{a}}}{\frac{1}{q_{\mathrm{sw}}\chi} + \frac{L_{\mathrm{w}}^{\mathrm{v}}\rho_{\mathrm{a}}}{K_{\mathrm{a}}T}\left(\frac{L_{\mathrm{w}}^{\mathrm{v}} M_{\mathrm{w}}}{R^* T} - 1\right)} \cdot \\ & \cdot \left\{ 1 - \frac{1}{2}\left(\frac{q_{\mathrm{v}}}{q_{\mathrm{sw}}} - 1\right)\left[\frac{\rho_{\mathrm{a}}\left(\frac{L_{\mathrm{w}}^{\mathrm{v}} M_{\mathrm{w}}}{R^* T} - 1\right)}{\frac{K_{\mathrm{a}}T}{q_{\mathrm{sw}}\chi L_{\mathrm{w}}^{\mathrm{v}}} + \rho_{\mathrm{a}}\left(\frac{L_{\mathrm{w}}^{\mathrm{v}} M_{\mathrm{w}}}{R^* T} - 1\right)}\right]^2 \left[1 + \frac{1 - 2\frac{L_{\mathrm{w}}^{\mathrm{v}} M_{\mathrm{w}}}{R^* T}}{\left(\frac{L_{\mathrm{w}}^{\mathrm{v}} M_{\mathrm{w}}}{R^* T} - 1\right)^2}\right] \right\},\end{aligned} \tag{31}$$

where D is the particle diameter, q_{v} the specific humidity of the environment, q_{sw} the saturation specific humidity over water at the environmental temperature and pressure,

T the environmental temperature, R^* the universal gas constant and M_w the molecular weight of water. For the ventilation parameter (F) the expression proposed in [19] is used:

$$F = 0.78 + Sc^{1/3} Re^{1/2}\,, \tag{32}$$

where Sc is the Schmidt number (constant = 0.6) and Re the Reynolds number, $Re = DV_\mathrm{t}\rho_\mathrm{a}/\mu_\mathrm{dif}$, V_t is the particle terminal velocity, μ_dif the dynamical molecular viscosity of air and V_t is determined by (20). To obtain the rate of the specific mass change for the whole hydrometeor spectrum, (31) is integrated on particle diameter including (32):

$$\mathrm{REVP} = \int_0^\infty \frac{1}{\rho_\mathrm{a}} \frac{\mathrm{d}m_\mathrm{EVP}}{\mathrm{d}t} N_\mathrm{R}(D_\mathrm{R})\mathrm{d}D_\mathrm{R}\,, \tag{33}$$

where the index "R" indicates rain particles. The definitive form of the equation for REVP is presented in appendix B.

iv) Sublimation and deposition growth of snow (SSBL)

The theoretical basis of the parametrization of this process is the same as for the previous one. Here too, a more accurate approximation of the vapour density on an ice particle surface (30) is applied instead of the usual approximation (29). Therefore, in the "snow case", the equation for mass rate of change is like (31), but with saturation specific humidity over ice (q_si) and sublimation latent heat (L_i^v). The equation for SSBL is the same as for REVP, but here the parameters N_0S, k_S, n_S, λ_S of solid hydrometeors are used. The equation is valid in sublimation and in deposition growth due to the member which depends on the saturating conditions.

v) Accretion of cloud water by rain (RACW)

All processes of accretion are described in the same way in the parametrization. When falling, a hydrometeor collects (accretes) cloud particles along its path inside a volume that is considered cylindrical. This collection process has a certain efficiency that is taken into account by the accretion coefficient. The mass growth rate of the collecting particle is

$$\frac{\mathrm{d}m_\mathrm{AC}}{\mathrm{d}t} = \rho_\mathrm{a} \frac{\pi}{4} D^2 V_\mathrm{t}(D) E q, \tag{34}$$

where E is the accretion coefficient and q the specific mass of accreted particles. By integration of (34) for the whole spectrum of rain particles, the following rate of accretion of cloud water by rain is obtained:

$$\mathrm{RACW} = \int_0^\infty \frac{1}{\rho_\mathrm{a}} \frac{\mathrm{d}m_\mathrm{RACW}}{\mathrm{d}t} = \frac{\frac{\pi}{4} N_\mathrm{0R} E_\mathrm{RW} k_\mathrm{R} \left(\frac{p_0}{p}\right)^{0.4} \Gamma\left(n_\mathrm{R}+3\right) q_\mathrm{cw}}{\lambda_\mathrm{R}^{n_\mathrm{R}+3}}\,, \tag{35}$$

where the value 0.6 is used for the accretion coefficient (E_RW).

vi) Accretion of cloud ice by snow (SACI)

$$\text{SACI} = \frac{\frac{\pi}{4} N_{0\text{S}} E_{\text{SI}} k_{\text{S}} \left(\frac{p_0}{p}\right)^{0.4} \Gamma\left(n_{\text{S}} + 3\right) q_{\text{ci}}}{\lambda_{\text{S}}^{n_{\text{S}}+3}}\,, \tag{36}$$

where $E_{\text{SI}} = 0.1$ is the coefficient of collection of cloud ice by snow [3].

vii) Accretion of cloud ice by rain (freezing rain) (RACI)

This process takes place at temperature $T < T_0$ ($T_0 = 273.15$ K), the collision of a rain particle with a cloud ice particle results in the freezing of the rain particle, *i.e.* in the formation of a solid hydrometeor.

$$\text{RACI} = \frac{\frac{\pi}{4} N_{0\text{R}} E_{\text{RI}} k_{\text{R}} \left(\frac{p_0}{p}\right)^{0.4} \Gamma\left(n_{\text{R}} + 3\right) q_{\text{ci}}}{\lambda_{\text{R}}^{n_{\text{R}}+3}}\,, \tag{37}$$

where $E_{\text{RI}} = 1$ is the accretion coefficient for this process [3].

viii) Accretion of cloud water by snow (riming) (SACW)

At temperature $T < T_0$ the collision of solid hydrometeors with cloud water droplets results in the riming of snow flakes. This is also an accretion-type process and is thus parametrised in the same way:

$$\text{SACW} = \frac{\frac{\pi}{4} N_{0\text{S}} E_{\text{SW}} k_{\text{S}} \left(\frac{p_0}{p}\right)^{0.4} \Gamma\left(n_{\text{S}} + 3\right) q_{\text{cw}}}{\lambda_{\text{S}}^{n_{\text{S}}+3}}\,, \tag{38}$$

where $E_{\text{SW}} = 1$ according to [3].

ix) Accretion of rain by snow (SACR)

The idea of this process parametrization is taken from the scheme of Marecal *et al.* [4], where the authors also considered accreting interaction between hydrometeors of different phases. At temperature $T < T_0$ the collision of liquid and solid precipitation particles leads to their merging (with a certain efficiency), with the freezing of the liquid drop, *i.e.* to the growth of the solid hydrometeor particle. The approximation of this accreting process is like the previous one, but since both colliding particles have a certain size distribution, eq. (34) takes a slightly different form:

$$\frac{\mathrm{d}m_{\text{SACR}}}{\mathrm{d}t} = \frac{\pi}{4} \left(D_{\text{S}} + D_{\text{R}}\right)^2 \left|U_{\text{ts}} - U_{\text{tR}}\right| q_{\text{R}} E_{\text{SR}}\,, \tag{39}$$

where $\mathrm{d}m_{\text{SACR}}/\mathrm{d}t$ is the rate of growth of snow particle mass due to rain particle absorption, D_{S} and D_{R} are snow and rain particle diameters, U_{tS} and U_{tR} snow and rain mass-weighted mean terminal fall velocities, and E_{SR} is the accretion coefficient and is equal to 1 [4]. After the double integration of (39) over D_{S} and D_{R} for the whole size spectrum of snow and rain particles, the following approximating equation is obtained:

$$\text{SACR} = \frac{\pi}{4} \frac{\left|U_{\text{tS}} - U_{\text{tR}}\right|}{\rho_{\text{a}}} E_{\text{SR}} N_{0\text{S}} N_{0\text{R}} a_{\text{R}}\,. \tag{40}$$

$$\cdot\left\{\frac{\Gamma\left(b_{\mathrm{R}}+1\right)\Gamma(3)}{\lambda_{\mathrm{R}}^{b_{\mathrm{R}}+1}\lambda_{\mathrm{S}}^{3}}+\frac{2\Gamma\left(b_{\mathrm{R}}+2\right)\Gamma(2)}{\lambda_{\mathrm{R}}^{b_{\mathrm{R}}+2}\lambda_{\mathrm{S}}^{2}}+\frac{\Gamma\left(b_{\mathrm{R}}+3\right)\Gamma(1)}{\lambda_{\mathrm{R}}^{b_{\mathrm{R}}+3}\lambda_{\mathrm{S}}}\right\}.$$

x) Melting of snow (SMLT)

This process is active at temperature $T \geqslant T_0$. Its parametrization is based on the hypothesis of equilibrium between heat diffusion flux onto the surface of a melting particle and heat absorption by fusion [11]. Accordingly, the rate of mass transformation from the solid to liquid phase is

$$\frac{\mathrm{d}m_{\mathrm{MELT}}}{\mathrm{d}t}=\frac{2\pi DK_{\mathrm{a}}F\left(T-T_0\right)}{L_{\mathrm{i}}^{\mathrm{w}}}, \tag{41}$$

where F is ventilation (the same as in the rain evaporation parametrization), and $L_{\mathrm{i}}^{\mathrm{w}}$ is the fusion latent heat. For the whole spectrum of melting snow particles the rate of the process is

$$\begin{aligned}\mathrm{SMLT}=&\frac{2\pi K_{\mathrm{a}}F\left(T-T_0\right)}{\rho_{\mathrm{a}}L_{\mathrm{i}}^{\mathrm{w}}}N_{0\mathrm{S}}\cdot\\&\cdot\left\{\frac{0.78\Gamma(2)}{\lambda_{\mathrm{S}}^{2}}+0.31Sc^{1/3}\left(\frac{k_{\mathrm{s}}\rho_{\mathrm{a}}}{\mu_{\mathrm{dif}}}\right)^{1/2}\left(\frac{p_0}{p}\right)^{0.2}\frac{\Gamma\left(\frac{n_{\mathrm{S}}}{2}+\frac{5}{2}\right)}{\lambda_{\mathrm{S}}^{\frac{n_{\mathrm{S}}}{2}+\frac{5}{2}}}\right\}.\end{aligned} \tag{42}$$

xi) Evaporation of melting snow (SMEV)

This process is active at temperature $T \geqslant T_0$: when the melting of snow particles occurs, the solid hydrometeors maintain their size and form but are covered by a liquid water layer. So, for the parametrization of this process, eq. (31) over the solid precipitation spectrum is integrated:

$$\mathrm{SMEV}=\int_0^\infty\frac{1}{\rho_{\mathrm{a}}}\frac{\mathrm{d}m_{\mathrm{EVP}}}{\mathrm{d}t}N_{\mathrm{S}}\left(D_{\mathrm{S}}\right)\mathrm{d}D_{\mathrm{S}}\,, \tag{43}$$

where index "S" indicates snow particles. The form of the equation for SMEV is presented in appendix B.

xii) Accretion of cloud water by melting snow (SMACW)

At temperature $T \geqslant T_0$ the interaction between cloud liquid water particles and melting snow particles contributes to the melting of snow because liquid droplets contain heat, which may be used by the melting process.

$$L_{\mathrm{i}}^{\mathrm{w}}\frac{\mathrm{d}m_{\mathrm{SMACW}}}{\mathrm{d}t}=C_{\mathrm{w}}\left(T-T_0\right)\frac{\mathrm{d}m_{\mathrm{SACW}}}{\mathrm{d}t}, \tag{44}$$

where $\frac{\mathrm{d}m_{\mathrm{SMACW}}}{\mathrm{d}t}$ is the melting mass-rate due to the present process. For all the snow particles the following equation is valid:

$$\mathrm{SMACW}=\frac{C_{\mathrm{w}}\left(T-T_0\right)}{L_{\mathrm{i}}^{\mathrm{w}}}\mathrm{SACW} \tag{45}$$

with SACW given by (38).

xiii) Accretion of rain by melting snow (SMACR)

As for the previous process, this accretion interaction also accelerates the snow melting at temperature $T \geqslant T_0$. Its parametrization is the same:

$$\text{SMACR} = \frac{C_{\text{w}}\,(T - T_0)}{L_{\text{i}}^{\text{w}}}\text{SACR}\,, \tag{46}$$

where SACR is given by (40).

Note that in processes RACI and SMACW the cloud ice or cloud water mass change involved in the process is neglected with respect to the hydrometeor mass change. Accordingly the rates of change of model variables by slow microphysical processes are

$$\frac{\partial q_{\text{v}}}{\partial t} = -\text{REVP} - \text{SSBL} - \text{SMEV}, \tag{47}$$

$$\frac{\partial q_{\text{cw}}}{\partial t} = -\text{RAUT} - \text{RACW} - \text{SACW}, \tag{48}$$

$$\frac{\partial q_{\text{ci}}}{\partial t} = -\text{SAUT} - \text{SACI}, \tag{49}$$

$$\frac{\partial q_{\text{R}}}{\partial t} = \text{RAUT} + \text{REVP} + \text{RACW} - \text{RACI} - \text{SACR} + \text{SMLT} + \\ + \text{SMACW} + \text{SMACR}\,, \tag{50}$$

$$\frac{\partial q_{\text{S}}}{\partial t} = \text{SAUT} + \text{SSBL} + \text{SACI} + \text{RACI} + \text{SACW} + \text{SACR} - \\ - \text{SMLT} + \text{SMEV} - \text{SMACW} - \text{SMACR}\,, \tag{51}$$

and the temperature rate of change due to slow microphysical processes is

$$\frac{\partial T}{\partial t} = \frac{L_{\text{w}}^{\text{v}}}{C_p^{\text{d}}}(\text{REVP} + \text{SMEV}) + \frac{L_{\text{i}}^{\text{v}}}{C_p^{\text{d}}}(\text{SSBL}) + \\ + \frac{L_{\text{i}}^{\text{w}}}{C_p^{\text{d}}}(\text{RACI} + \text{SACW} + \text{SACR} - \text{SMLT} - \text{SMACW} - \text{SMACR})\,. \tag{52}$$

Since the fast microphysical process parametrization uses the variable $q = q_{\text{v}} + q_{\text{cw}} + q_{\text{ci}}$, the rate of change of this variable due to slow processes can be obtained by adding eqs. (47), (48) and (49). Equations (50) and (51) provide the values for $M_{\text{R}}^{\text{v,c}}$ and $M_{\text{S}}^{\text{v,c}}$, correspondingly, in (7), (8), (9).

5. – Results of the microphysical parametrization verification with the two-dimensional cumulonimbus model

A two-dimensional cumulonimbus model [7] is used for the verification of the microphysical parametrization. A brief description of that model is presented here. The model is based on the deep convection (quasi-Boussinesq) equations (anelastic, non-hydrostatic) [20], with a simple parametrization of turbulent (viscous) members, and a

TABLE II. – *List of initial data used in the numerical experiment. Vertical size of the domain, vertical limits of initial humidity perturbation, points and dates of radiosounding, literature sources of the initial data.*

Case number	Site and date of radiosounding	Bibliographic source of the observation	Vertical size of the model domain (km)	Vertical limits of the initial humidity perturbation (km)
I	Miles City (USA) 19 July 1981	[21]	10	1–2.5
II	Miles City (USA) 1 August 1981	[22]	14	2.5–5
III	Knowlton (USA) 2 August 1981	[23]	14	0.5–1.75
IV	Denver (USA) 11 July 1988	[24]	10	1.5–5
V	Denver (USA) 14 July 1982	[25]	10	5.25–7.75
VI	Denver (USA) 17 July 1987	[26]	10	1–2.75
VII	Redstone (USA) 20 July 1986	[27]	14	1.5–5
VIII	Sterling (USA) 22 June 1976	[28]	14	1.75–4.25
IX	Penhold (Canada) 26 July 1983	[29]	10	0.75–3.75

predictor-corrector time-stepping numerical scheme (prediction step is implicit, correction step is explicit). A simple geometric grid for the numerical solution is used. The experiments are performed with a resolution of 250 m on the horizontal and vertical axes. The simulation domain size is 20 km along the horizontal axis and 10–14 km along the vertical axis. Over lateral boundaries the periodicity condition is applied, while different radiosounding observations are used as initial condition, with the addition of a humid bubble, which is a non-hydrostatic humidity perturbation in the layer close to saturated conditions, in order to bring about convective motion. A time step equal to 5 s is used.

This numerical model with the proposed microphysical parametrization has been tested by running nine experiments using the radiosounding data published in the literature for cumuloninbus cases (see table II).

The simulations were carried out for one hour, which is the typical lifetime of a cumulonimbus. These simulations were performed for two purposes: the general microphysical parametrisation verification and the estimation of the effect of using a more accurate approximation of the evaporation and sublimation of precipitation particles (see sect. **4**). Some simulation results are presented in table III. On the base of this table, comparisons can be made and some conclusions can be drawn.

The comparison between the simulation results and the available observations of the thermodynamic features of deep-convection shows that these are successfully reproduced by the cumulonimbus model. The same is true also for the total water content (of cloud and precipitation). For every case, detailed information on doppler-radar reflectivity is available. This parameter is very useful for estimating condensed water content and precipitation distribution at the ground. The radar reflectivity is estimated also from the

TABLE III. – *Parameters of humid convection with the observation data, the calculations from the observation data and the numerical experiment results*([1]).

Humid convective parameter	Case number	Observation data and parameter valued from observation data	Numerical experiment with the first parameterization scheme([2])	Numerical experiment with the second parameterization scheme([3])
1	2	3	4	5
Maximum value of updraft speed (ms^{-1})	I	15	19.6	19.6
	II	37	35.7	35.7
	III	55	41.8	42.3
	IV	–	43.1	43.0
	V	14	19.8	–
	VI	13	23.1	23.1
	VII	25	17.8	–
	VIII	14	19.3	19.4
	IX	25.2	22.4	22.5
Maximum value of downdraft speed (ms^{-1})	I	3	8.2	–
	II	9	11.0	–
	III	10	22.6	–
	IV	–	23.7	–
	V	13	9.0	–
	VI	6	16.1	–
	VII	15	9.5	–
	VIII	9	10.0	–
	IX	13.5	8.6	–
Maximum perturbation of temperature (K)	I	2.5	10.2	10.2
	III	11.0	14.3	14.6
	II	19.0	24.0	24.2
	IV	7.0	10.0	10.0
	V	–	6.1	–
	VI	–	11.9	11.9
	VII	7.0	10.3	–
	VIII	–	7.3	7.3
	IX	–	9.4	9.4
Maximum value of total water content (of cloud and precipitation) ($kgkg^{-1}$)	I	0.5×10^{-2}	1.03×10^{-2}	1.33×10^{-2}
	II	0.9×10^{-2}	0.84×10^{-2}	1.28×10^{-2}
	III	1.12×10^{-2}	1.12×10^{-2}	1.93×10^{-2}
	IV	–	0.80×10^{-2}	1.14×10^{-2}
	V	–	0.54×10^{-2}	–
	VI	–	1.87×10^{-2}	2.29×10^{-2}
	VII	–	2.01×10^{-2}	–
	VIII	1.5×10^{-2}	0.88×10^{-2}	1.36×10^{-2}
	IX	–	0.93×10^{-2}	1.19×10^{-2}
Maximum value of cloud specific mass ($kgkg^{-1}$)	I	–	0.27×10^{-2}	0.28×10^{-2}
	III	–	0.44×10^{-2}	0.44×10^{-2}
	II	–	0.33×10^{-2}	0.33×10^{-2}
	IV	–	0.40×10^{-2}	0.40×10^{-2}
	VI	–	0.37×10^{-2}	0.37×10^{-2}
	VIII	–	0.32×10^{-2}	0.33×10^{-2}
	IX	–	0.28×10^{-2}	0.28×10^{-2}

TABLE III. – *Continued.*

1	2	3	4	5
Maximum value of precipitation specific mass (kgkg^{-1})	I	–	1.01×10^{-2}	1.05×10^{-2}
	III	–	0.84×10^{-2}	0.84×10^{-2}
	II	–	1.62×10^{-2}	1.60×10^{-2}
	IV	–	0.80×10^{-2}	0.74×10^{-2}
	VI	–	1.87×10^{-2}	1.92×10^{-2}
	VIII	–	0.91×10^{-2}	1.03×10^{-2}
	IX	–	0.92×10^{-2}	0.91×10^{-2}
Maximum value of radar reflectivity (dBz)	I	57	56	–
	II	63	35	–
	II	62	61	–
	IV	50	46	–
	V	48	48	–
	VI	56	59	–
	VII	65	58	–
	VIII	72	38	–
	IX	57	54	–
Maximal value of radar reflectivity on the ground surface (dBz)	I	57	41	–
	II	55	No	–
	II	59	43	–
	IV	No	29	–
	V	40	No	–
	VI	53	42	–
	VII	50	43	–
	VIII	65	No	–
	IX	57	36	–
Accumulated precipitation at the ground (mm)	I	–	1.86	–
	II	–	0	–
	II	–	2.52	–
	IV	0	0	–
	V	–	0	–
	VI	11	1.52	–
	VII	–	1.70	–
	VIII	–	0	–
	IX	–	0.57	–
Maximum intensity of precipitation at the ground (mmh^{-1})	I	–	33.24	35.84
	III	–	0	0.03
	II	–	110.76	100.11
	IV	–	0	5.02
	VI	–	18.23	21.82
	VIII	–	0	1.34
	IX	–	0.56	40.18

([1]) Absence of data is indicated by the dash symbol.
([2]) The microphysical parametrization with more accurate method of hydrometeor evaporation (sublimation) approximation.
([3]) The microphysical parametrization with the traditional method of hydrometeor evaporation (sublimation) approximation.

simulation results using a standard method of reflectivity calculation from precipitation parameters [30,31]. In table III we can see that the modelled precipitation fields, such as diagnosed reflectivity, are very close to observed values. It is therefore possible to affirm that the model with the above-described microphysical parametrization is in condition to realistically reproduce atmospheric precipitation fields. Unfortunately, there are insufficient data on accumulated precipitation at the ground for verifying the model's capacity to simulate this parameter.

According to theoretical reasoning, the use of the more accurate method of the approximation of hydrometeors evaporation and sublimation could lead to a more reliable representation of these processes when they are very intense. To verify this hypothesis, some experiments have been repeated, exchanging the evaporation/sublimation parametrization used in this work by the traditional method.

The two series of experiments provided similar values of humid convection microphysical parameters, although the rates of evaporation and sublimation of hydrometeors are remarkably different. Comparing maximum values within the domain (fig. 2), we see that the more accurate method produces values of evaporation up to 10 times larger and values of sublimation up to 20 times larger with respect to the "traditional method". Of course, this difference is mainly present in the stages of maximum development of these microphysical processes, but also outside these stages the difference between evaporation and sublimation rates obtained by the two methods is marked (not less than 3 times).

Table III shows that the results achieved by both methods of hydrometeors evaporation/sublimation parametrization are in fact very close to each other; there are practically no differences between the values of updraft speed, temperature perturbation and cloud specific mass. The difference between these two experimental series appears in the values of precipitation specific mass and those of ground accumulated precipitation and precipitation rate: the traditional method obtained more intense precipitation in comparison with the more accurate one in 6 out of 7 cases. It is not possible to draw a clear conclusion for the accumulated precipitation because this datum is available only for a limited number of cases (table III). Nonetheless, it can be said that the traditional method has the tendency to overestimate the accumulated precipitation.

From the theoretical and numerical studies, it is known that, with unstable background conditions, humid convection has a tendency to repeat its life cycle several times in the case of two-dimensional simulation, because of an absence of dynamical energy dissipation. The fact that the proposed two-dimensional model, with unstable background conditions and in the absence of a background wind, can reproduce the effect of periodic development of convection, indicates that the model adequately reproduces the phenomenon of atmospheric convection and can be a suitable tool for testing and studying thermodynamical and microphysical processes. Therefore, for general verification of the proposed parametrization, the life cycle of a cumulonimbus reproduced by the model simulation has been examined. The case of Denver, 11 July 1988 (see table II), has been chosen for this purpose.

The first stage of the convection evolution is characterised by the acceleration of convective motions and continues until the appearance of maximum values of updraft, approximately 30 minutes after the triggering of convection. During this stage the cloud is already formed and the maximum value of cloud water content is found. Figure 3 shows that the largest part of the cloud is formed by the crystal phase of condensate because the cloud is situated between 4 and 10 km (*i.e.* at low temperature, between -5 and $-40\,^{\circ}\mathrm{C}$). One can also see that, at the end of this stage of maximum dynamical activity, the cloud spreads along the top boundary on the upper levels forming the anvil

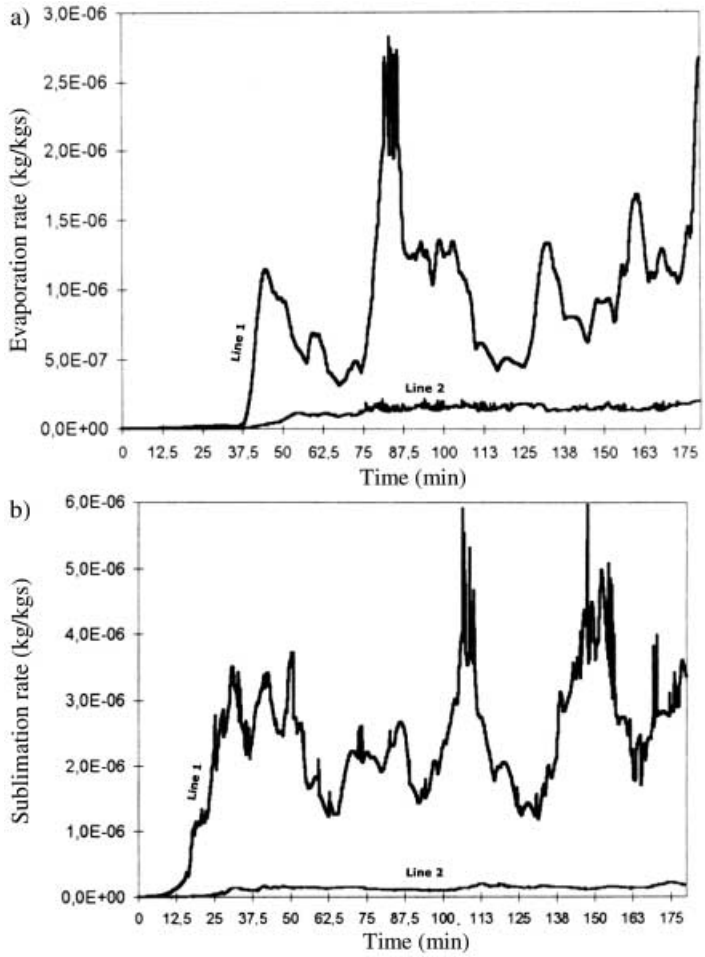

Fig. 2. – Time change of the maximum (for the model domain) value of the rate of liquid hydrometeor evaporation (a) and solid hydrometeor sublimation (b) obtained from the numerical experiment with the initial data of the radiosounding in Denver, 11 July 1988. The different methods used in this process approximation: Line 1: the more accurate method, Line 2: the traditional method.

which is typical of cumulonimbus clouds. The top boundary has the role of constraining layer, replacing the effect of tropopause.

The second stage of the cloud evolution is characterised by the slowing down of the updraft and demolition of the cloud. This stage continues up to 50 minutes after convection triggering (fig. 4). At this stage the cloud divides into two separated parts which are in areas of moderate updraft flows, while a strong downdraft jet is formed in the centre of the domain. As in the first stage, intense development of microphysical processes is also observed. Thus, at the end of the second stage precipitation is formed, although maximum values of its water content appear at the following stage.

The third and final stage of the life cycle of a cumulonimbus takes place more or less between 50 minutes and 1.5 hours after triggering of convection. During this stage

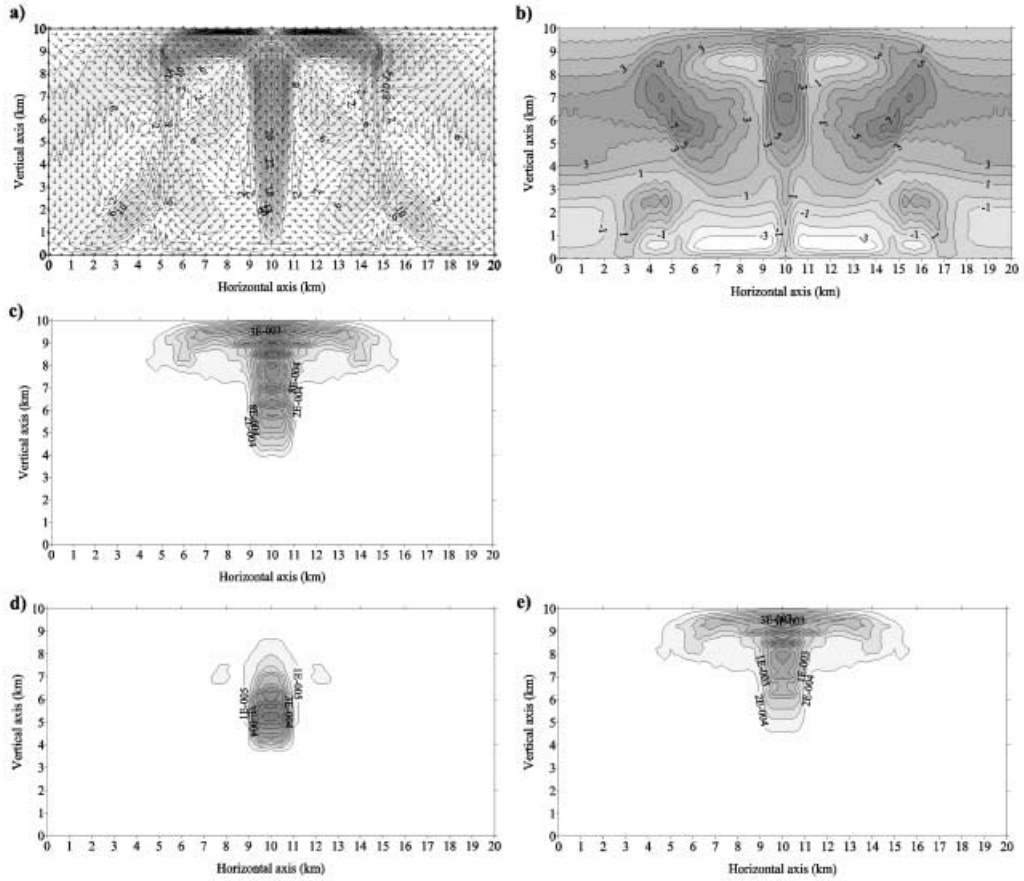

Fig. 3. – Model variable fields obtained from the numerical experiment with initial data of the radiosounding in Denver (USA), 11 July 1988, 30 minutes after convection triggering: a) air velocity field (isolines, m/s) and jet directions (arrows); b) temperature perturbation field (K), c) field of total cloud condensate specific mass (kg/kg); d) field of liquid cloud condensate specific mass (kg/kg); e) field of ice cloud condensate specific mass (kg/kg).

the maximum development of the precipitation field is reached and a very interesting transition to a new life cycle in the dynamical regime is observed. In fact, fig. 5 shows the situation after 1 hour from the initial motion, with the signs of a new cycle appearing in the low levels below the cloud: several new jets of updraft. Later on, this complex dynamical structure evolves into a structure which is very similar to the one appearing during the first stage of the cumulonimbus life cycle, *i.e.* the central updraft jet is intensified at the same time as the lateral jets disappear (after about 1.5 hours). At this stage, cloud condensate almost completely disappears and the precipitation reaches a peak in its development. In spite of the high values of its specific mass field (the maximum is $7 \times 10^{-3}\,\mathrm{kgkg}^{-1}$), the precipitation does not fall to the ground due to the intense evaporation taking place in the layer below the cloud, in agreement with observations. At the end of this stage a new convective updraft is formed and a new cloud appears. This means that a new cycle has begun.

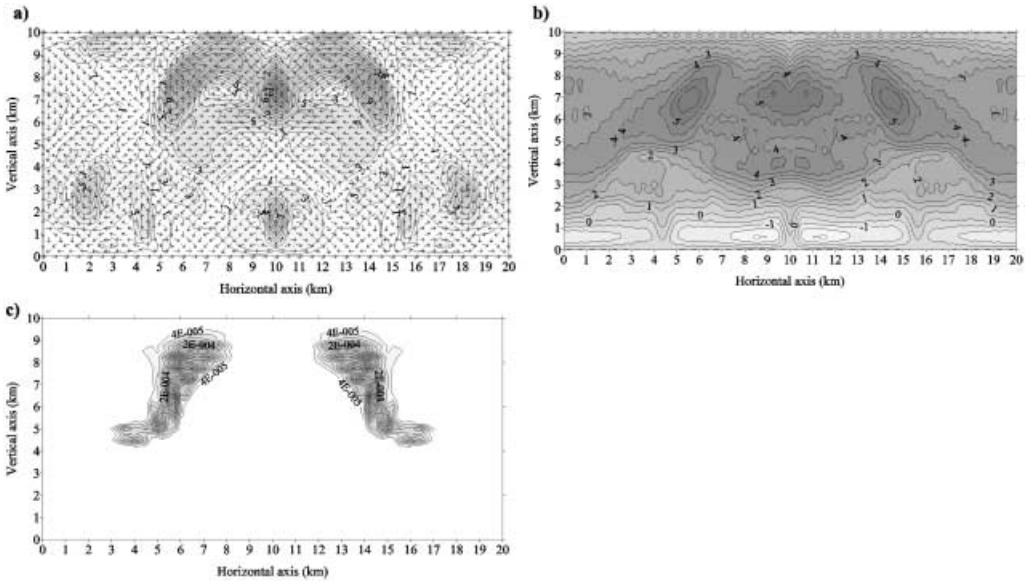

Fig. 4. – Same as fig. 3, but for 50 minutes after convection triggering: a) air velocity field (isolines, m/s) and jet directions (arrows); b) temperature perturbation field (K), c) field of total cloud condensate specific mass (kg/kg).

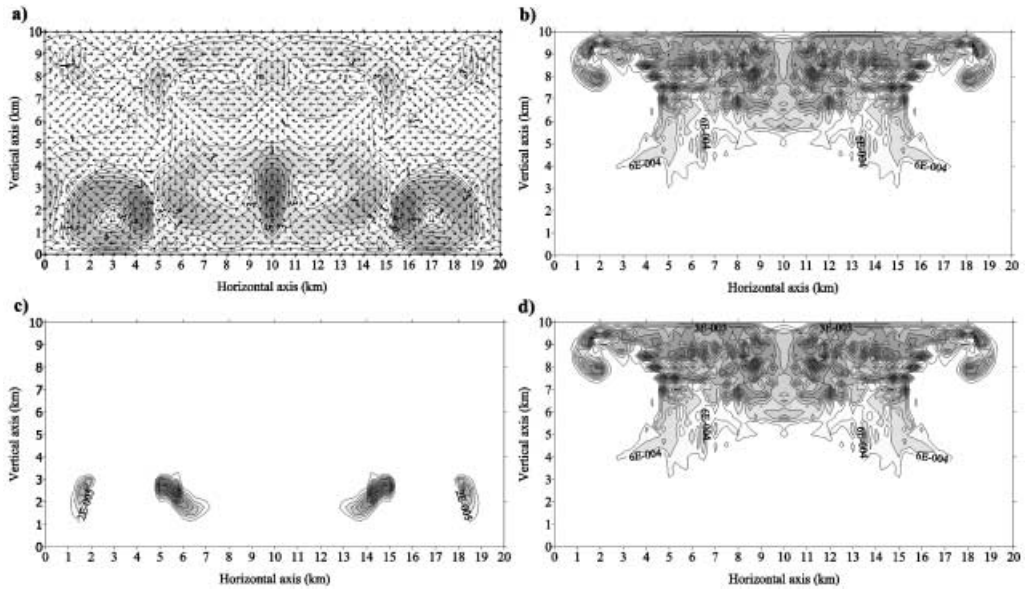

Fig. 5. – Same as fig. 3, but for 1 hour after convection triggering: a) air velocity field (isolines, m/s) and jet directions (arrows); b) field of total precipitation condensate specific mass (kg/kg); c) field of liquid precipitation condensate specific mass (kg/kg); d) field of solid precipitation condensate specific mass (kg/kg).

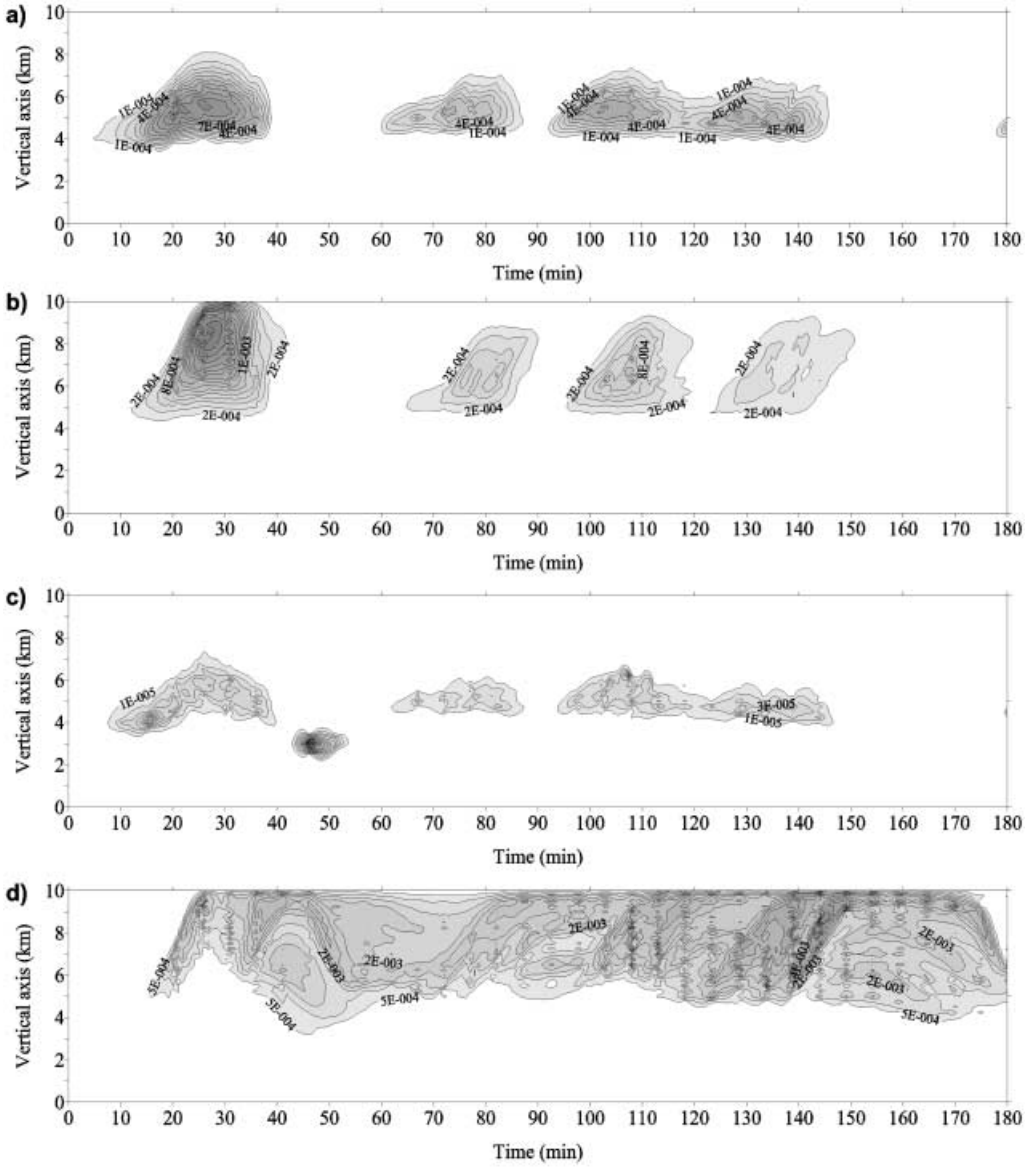

Fig. 6. – Isopleths of the profiles of cloud water (a), cloud ice (b), liquid precipitation (c) and solid precipitation (d) specific mass (kg/kg) from the results of the numerical experiment with initial data of the radiosounding in Denver (USA), 11 July 1988. The profiles belong to the centre of the model domain.

The evolution of the microphysical processes is analysed below on the basis of the study of cloud and precipitation parameter profiles during a 3 hour integration. A good way to visualise these quantities is through contour plots with time coordinate on the horizontal axis and (vertical) space coordinate on the vertical axis. Panels a) and b) of fig. 6 show that cloud was formed 4 times during 3 hours, approximately on the same

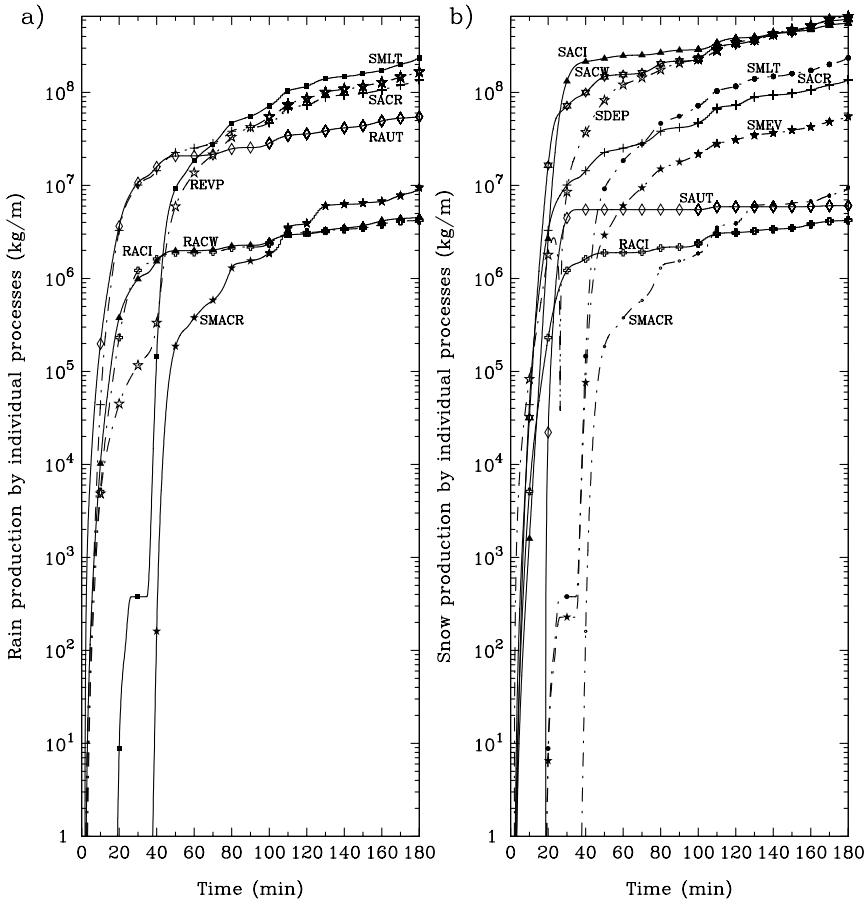

Fig. 7. – Space-integrated accumulated production of liquid (a) and solid (b) precipitation mass (kg/m) by individual microphysical processes (positive contribution is indicated by the solid line and negative contribution by the dashed line) from the results of the numerical experiment with initial data of the radiosounding in Denver (USA), 11 July 1988.

vertical layer, the 4 cycles are clearly visible. At the same time panels c) and d) of fig. 6 show that the limits of each life cycle of precipitation are less distinct because their evolution is determined by slower microphysical processes.

The analysis of the contribution of various microphysical processes to the evolution of the precipitation specific mass field allows us to draw some conclusions about the relative importance of the separate processes. For this purpose, the space-integrated production of precipitation mass by means of each microphysical process will be analysed (fig. 7).

The autoconversion of rain is one of the most important processes in rain formation, especially at the initial stage, while for snow formation it is not so crucial. Sublimation makes the largest contribution to snow decrease, as this process is fast and intensive. In rain evolution the evaporation process plays a significant role on a long time scale, but its contribution to rain decrease is weaker in comparison to the sublimation of snow. The next process group includes the following subgroups of microphysical processes: i) accretion increasing rain mass, ii) accretion increasing snow mass, iii) accretion decreasing

rain mass, iv) accretion decreasing snow mass. The role of accretion in the increase of rain mass (RACW and SMACR) is important only on limited stages of the evolution of cumulonimbus. Conversely, for snow increase this process subgroup (SACI, SACW, SACR, RACI) plays the most significant role during all the integration. The opposite situation is found for the role of accretion in precipitation decrease: for rain it makes a valuable contribution (SACR, RACI), while for snow (SMACR) it is unessential. Finally, concerning snow melting, it can be seen that apart from the initial stage, when not enough snow has reached the area with positive temperature, it is the main contributor to rain formation, but not the main contributor to snow decrease, sublimation being stronger here.

Thus the above showed that all microphysical processes are important in different stages of cumulonimbus life and that the microphysical parametrization does not include "unnecessary" processes.

6. – Results of the microphysical parametrization verification with the BOLAM model

The BOLAM model has been developed at the Institute of Atmospheric and Climate Sciences of the Italian National Research Council (ISAC-CNR, Bologna, Italy) [32-35]. BOLAM is a hydrostatic, primitive-equation, gridpoint model. The horizontal grid is based on geographical coordinates on a rotated Arakawa C grid, where the rotated equator is located at the mid-latitude of the model domain to minimise grid anisotropy. The model includes the following subgrid scale process parametrization schemes: boundary layer scheme, convection (Kain-Frisch) scheme [36], three-layer soil model, radiation scheme, water cycle scheme [37] partly based on the simplified microphysical parametrization of Schultz [8]. Water cycle scheme has five explicit prognostic variables: cloud ice, cloud water, rain, snow and graupel; the microphysical processes are parametrized as a function of the local thermodynamic variables and the concentration of condensate. BOLAM has several space-resolution variants with a nesting procedure connecting them.

In this model the contribution of microphysical processes parametrization to simulation results is smaller compared to the simplified two-dimensional cumulonimbus model. Nonetheless, the attempt to apply the new scheme can be useful in estimating its suitability for this model type and in evaluating the effect in comparison with a Schultz-type parametrization.

For this study a numerical simulation of a very strong rainfall case in the Alpine Region, the 1994 Piedmont flood, has been performed. For that episode the heaviest rainfall was observed over northern Italy. Simulations of 24 hours integration with BOLAM for the 5 November 1994 were made. A detailed description of this case with the presentation of observed data can be seen in the work of Buzzi, Tartaglione, Malguzzi [38].

The simulation with BOLAM was carried out with 10 km horizontal space resolution and 36 vertical levels. The initial and boundary condition values are taken from the results of integration with the BOLAM version with 30 km horizontal resolution and 30 vertical levels by the nesting procedure. In its turn the initial and boundary conditions for the "large" BOLAM are obtained from ECMWF initialised 6-hourly analyses at 0.75° resolution on 15 standard pressure levels by an interpolating procedure. The initial data were taken on 0000 UTC 5 November 1994.

Two numerical experiments were performed with the two microphysical parametrizations: one with the parametrization based on the Schultz scheme (BME) and one with the new parametrization (NME). On the basis of the simulation results, the following

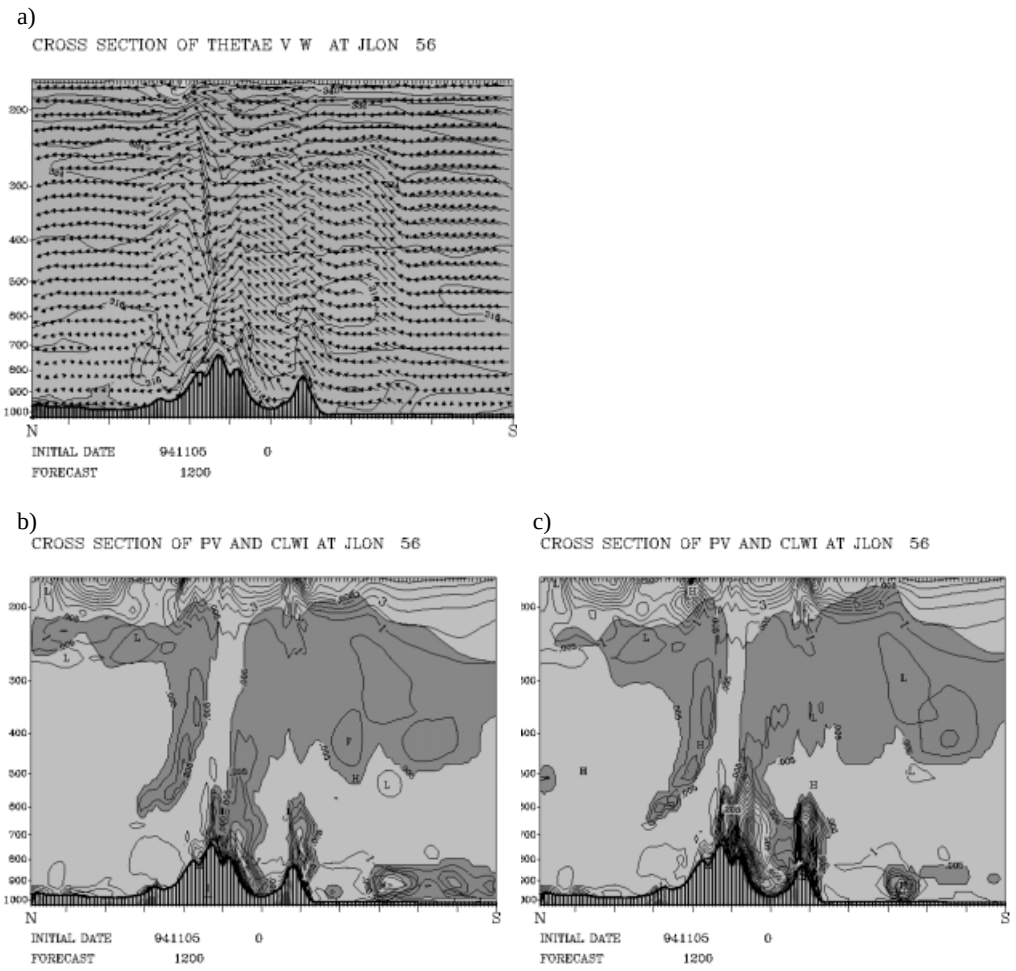

Fig. 8. – Latitudinal cross-sections along 7.4° E of the model domain with the predicted fields after 12 hours of simulation in BME and in NME: a) zonal air flow with scaled arrows and potential temperature (K) with isolines (every 4K); b) total cloud specific mass (g/kg) with isolines (every 0.1 g/kg) and with filled contour dark intensity in BME; c) same as b) for NME.

conclusions can be drawn. First, the change in microphysical scheme had practically no influence on the dynamics, *i.e.* the thermodynamical model fields remained virtually unaltered. Secondly, for the fields of model microphysical parameters, some interesting results were obtained: the new microphysical parametrization significantly changed cloud water content fields and, correspondingly, accumulated fallen precipitation field.

To extract information on variations in the microphysical parameters, the cloud water content fields can be analysed. These fields are presented as longitudinal and latitudinal domain cross-sections after 12 h of simulation (the moment when the dynamical and microphysical processes were very active). Figures 8 and 9 present the fields of the following parameters: the air flow component parallel to the section plane is presented by arrows (fig. 8a, 9a); potential temperature (fig. 8a, 9a) by isolines; total cloud specific

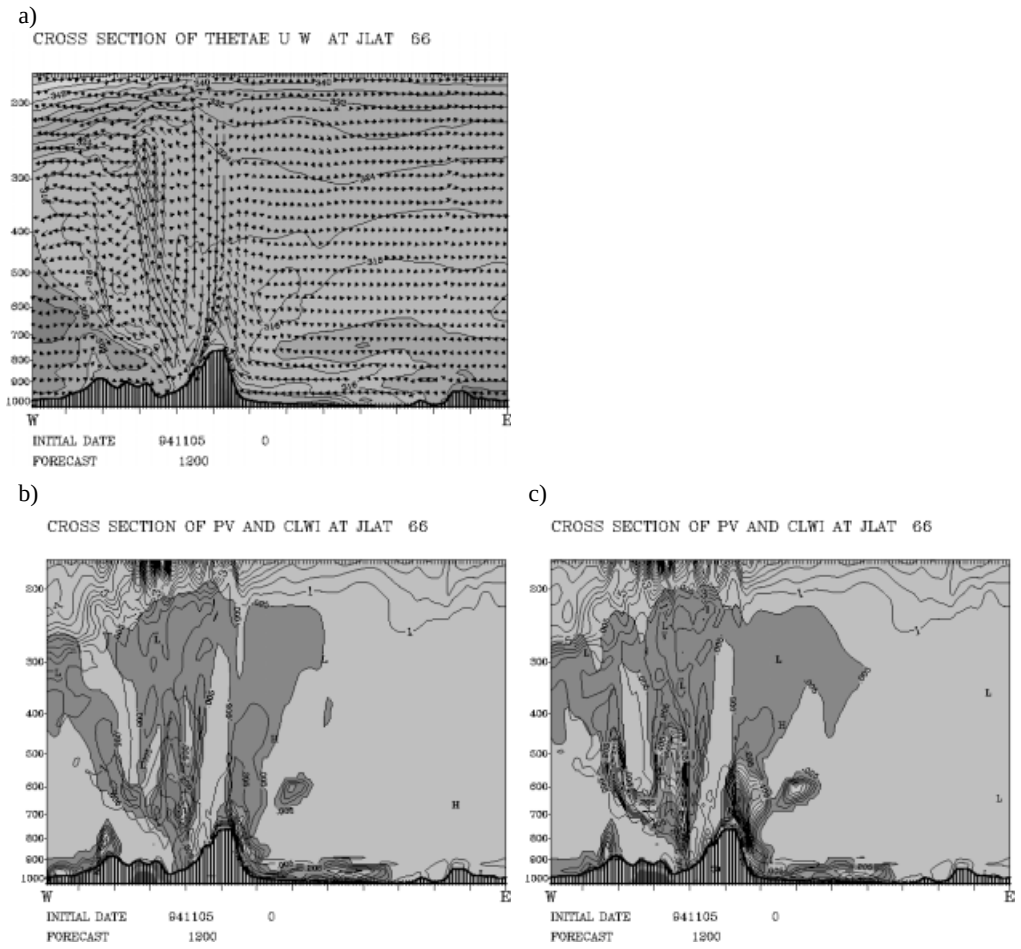

Fig. 9. – Longitudinal cross-section along 45.2° N of the model domain with the predicted fields after 12 hours of the simulation in BME and in NME: a) meridional air flow with scaled arrows and potential temperature (K) with isolines (every 4K); b) total cloud specific mass (g/kg) with isolines (every 0.1 g/kg) and with fill contour dark intensity in BME; c) same as b) for NME.

mass (fig. 8b, 8c, 9b, 9c) by thin isolines and dark intensity; potential vorticity (fig. 8b, 8c, 9b, 9c) by thick isolines. Figure 8 reveals that, on the background of an intense southerly flow, strong vertical flows developed under the influence of the orography. In the zone of updraft, an extensive and strong cloud system forms in both experiments. The spatial form of this cloud system from BME and from NME is very similar, but the values of cloud water content are essentially different. In the BME case the local maximum of cloud specific mass field close to the southern Alpine slope is $0.71\,\mathrm{gkg}^{-1}$, while in the NME case this maximum is $1.55\,\mathrm{gkg}^{-1}$. The same situation occurs with the maximum located on the southern Ligurian Apennines slope: $0.70\,\mathrm{gkg}^{-1}$ in the BME case and $1.46\,\mathrm{gkg}^{-1}$ in the NME case. In addition, in NME the large cloud system of the low and middle atmospheric layers does not have a gap between the two mountain ranges, but only a local minimum of cloud water content. This fact may be explained

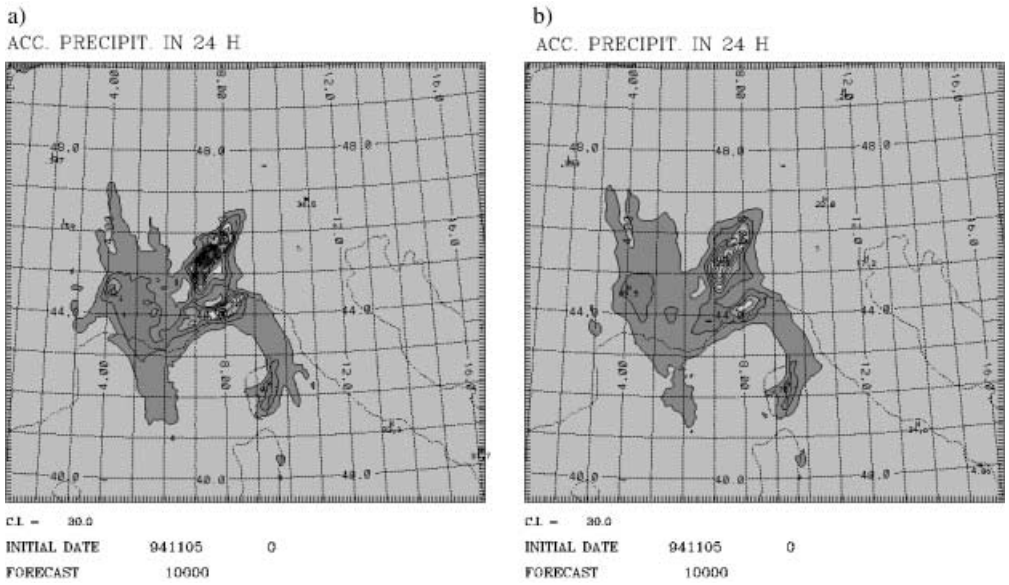

Fig. 10. – Fields of the 24 h accumulated simulated fallen precipitation (mm): a) in BME and b) in NME. Contours every 30 mm.

in terms of the greater values of cloud specific mass obtained in NME, due to the higher efficiency of "rapid" microphysical processes; the gap in the cloud system is absent in NME because the high values of cloud water content, which are formed on the first updraft experienced by the flow (see fig. 8a), are too large to disappear completely in the subsequent downdraft conditions, as occurs in BME. In conditions of intensive downdraft in the west of Alps, which are presented in the longitudinal cross-section (fig. 9), the great values of cloud water content also disappear in NME.

The 24 h accumulated precipitations in BME and NME are shown in fig. 10. There are some important differences between these fields. The first regards the maximum values: in BME it is $400\,\mathrm{mm(24h)^{-1}}$ and in NME it is $255\,\mathrm{mm\,(24h)^{-1}}$, while the observed maximum value, the position of which is very close to the simulated position, is $292\,\mathrm{mm\,(24h)^{-1}}$ [38]; this maximum is located in the Piedmont region on the southern Alpine slope. The next local maximum of precipitation was observed in the Liguria region, on the northern Apennine slope. In this location, the BME simulates 210 mm of fallen precipitation, which is closer to the observed value (250 mm) than the one simulated by NME (160 mm). At the same time NME did not predict a gap in the precipitation field between the two mentioned maxima, while it gave a local minimum only, which is more realistic than the gap with no precipitation at all, shown by BME. It can be said, in general, that the use of this more accurate parametrisation of microphysical processes results in that the model produces a precipitation field which is smoother and extends more realistically on the downwind slope of the orography, while a typical systematic error of mesoscale atmospheric models is the precipitation field highly peaked over the orography maxima and confined to the windward slope of the mountains.

Naturally, such numerical experiments do not allow us to draw any definite conclusion regarding the effect obtained in BOLAM by the insertion of the microphysical

parametrization discussed in this paper. However, the attempt to make this insertion turns out to be successful. It shows that the microphysical parametrization can be used also in complex atmospherical models, like BOLAM, and it provides changes in the simulation results, which regard cloud and precipitation field features, in comparison to the parametrization of Schultz.

7. – Conclusions

The present work proposed a parametrization of the microphysical atmospherical processes intended to be used in numerical models of different spatial scales and resolutions. The parametrization includes some well-known hypotheses as well as methods with new elements, with regard to the general scheme organisation and to the approximation of some microphysical processes. The parametrization is based on the original assumption of the thermodynamical equilibrium, which, in turn, is based on the entropy conservation law in a closed thermodynamical system. The parametrization proposes an unusual method of dividing the atmospheric microphysical processes into two groups, which are approximated with two methods based on different principles. It provides a complete set of process approximations, starting from water and ice cloud condensate formation and ending up with liquid and solid precipitation fall. The parametrization is an attempt to reproduce the very complex atmospheric water evolution, but remains generalised and uncomplicated so that it can be used in a varied spectrum of models, from a simplified numerical atmospheric model to an operational weather forecast model.

The proposed parametrization is verified in two very different numerical models: in a two-dimensional nonhydrostatic cumulonimbus model and in the weather forecast model BOLAM.

The verification with the cumulonimbus model provided information on the parametrization's ability to reproduce basic cumulonimbus parameters. It has been possible also to make an estimation of the effects obtained by introducing some new, more precise, parametrization elements. It is, in fact, demonstrated that such elements can be useful and more satisfactory. Moreover, the experimental results obtained with the mentioned model show that a simplified microphysical parametrization which does not include the solid phase of the atmospheric condensate cannot be considered satisfactory in a model of this type. The model results also induced us to analyse the cumulonimbus life cycle and the role played by the groups of microphysical processes included in the parametrization. This analysis shows that all of the considered processes make an important contribution to the cloud and precipitation evolution.

For parametrization verification with BOLAM, an experiment for the 1994 Piedmont flood case has been simulated. Some comparisons are made between the simulation results obtained with the previous BOLAM microphysical parametrization and those from the parametrization presented here. The verification demonstrates that the proposed parametrization can also be used successfully in an operational model.

* * *

The author wishes to thank Dr. D. Ya. Pressman of the Hydrometeorological Centre of Russia for his valuable help in setting up the two-dimensional cumulonimbus model. Discussions of the parametrization verification with the cumulonimbus model with Prof. N. F. Veltish'ev of the Moscow State University were very useful. The parametrization verification with BOLAM was performed with the great assistance of its authors, A. Buzzi and P. Malguzzi (ISAC, CNR, Italy). This study has been supported

by the Russian Hydrometeorological Research Centre, the Hydrometeorological Centre of Russia, and the projects in the CNR of Italy: EC Project RAPHAEL (ENV4 –CT97-0552), CNR-GNDCI Project "Sensori Remoti e Precipitazioni Estreme".

Appendix A.

List of physical constants

C_p^{d}	Specific heat of dry air vapour at constant pressure	1004.7	$\mathrm{Jkg^{-1}K^{-1}}$
C_p^{v}	Specific heat of water vapour at constant pressure	1846.0	$\mathrm{Jkg^{-1}K^{-1}}$
C_{i}	Specific heat of ice	2093.4	$\mathrm{Jkg^{-1}K^{-1}}$
C_{w}	Specific heat of water	4186.8	$\mathrm{Jkg^{-1}K^{-1}}$
E_{RI}	Coefficient of accretion of cloud ice by rain	1.0	
E_{RW}	Coefficient of accretion of cloud water by rain	0.6	
E_{SI}	Coefficient of accretion of cloud ice by snow	0.1	
E_{SR}	Coefficient of accretion of rain by snow	1.0	
E_{SW}	Coefficient of accretion of cloud water by snow	1.0	
K_a	Thermal conductivity of air	2.43×10^{-5}	$\mathrm{Jm^{-1}s^{-1}K^{-1}}$
$L_{\mathrm{i}}^{\mathrm{v}}$	Latent heat of water sublimation	2834170.5	$\mathrm{Jkg^{-1}}$
$L_{\mathrm{i}}^{\mathrm{w}}$	Latent heat of water fusion	333560.5	$\mathrm{Jkg^{-1}}$
$L_{\mathrm{w}}^{\mathrm{v}}$	Latent heat of water condensation	2500610.0	$\mathrm{Jkg^{-1}}$
M_{w}	Molecular weight of water	18.016	$\mathrm{kgkmol^{-1}}$
$q_{\mathrm{ci}}^{\mathrm{th}}$	Threshold value of cloud ice specific mass for its autoconversion	1×10^{-3}	$\mathrm{kgkg^{-1}}$
$q_{\mathrm{cw}}^{\mathrm{th}}$	Threshold value of cloud water specific mass for its autoconversion	5×10^{-5}	$\mathrm{kgkg^{-1}}$
R^*	Universal gas constant	8314.0	$\mathrm{Jkmol^{-1}K^{-1}}$
R_{d}	Gas constant of dry air	287.05	$\mathrm{Jkg^{-1}K^{-1}}$
R_{v}	Gas constant of water vapour	461.4	$\mathrm{Jkg^{-1}K^{-1}}$
Sc	Schmidt number	0.6	
α_{auti}	Rate coefficient of cloud ice autoconversion	1×10^{-3}	$\mathrm{s^{-1}}$
α_{autw}	Rate coefficient of cloud water autoconversion	1×10^{-3}	$\mathrm{s^{-1}}$
χ	Coefficient of molecular diffusion of vapour into air	2.26×10^{-5}	$\mathrm{m^2s^{-1}}$
μ_{dif}	Dynamical molecular viscosity of air	1.718×10^{-5}	$\mathrm{kgm^{-1}s^{-1}}$
π		3.1416	

Appendix B.

Approximation equations of the rate of some slow microphysical process

The evaporation rate of liquid hydrometeors (REVP)

$$\text{(A.1)}\quad \mathrm{REVP} = \frac{2\pi\left(\frac{q_{\mathrm{v}}}{q_{\mathrm{sw}}} - 1\right)}{\frac{1}{q_{\mathrm{sw}}\chi} + \frac{L_{\mathrm{w}}^{\mathrm{v}}\rho_{\mathrm{a}}}{K_{\mathrm{a}}T}\left(\frac{L_{\mathrm{w}}^{\mathrm{v}}M_{\mathrm{w}}}{R^*T} - 1\right)}\,.$$

$$\cdot\left\{1-\frac{1}{2}\left(\frac{q_{\mathrm{v}}}{q_{\mathrm{sw}}}-1\right)\left[\frac{\rho_{\mathrm{a}}\left(\frac{L_{\mathrm{w}}^{\mathrm{v}}M_{\mathrm{w}}}{R^{*}T}-1\right)}{\frac{K_{\mathrm{a}}T}{q_{\mathrm{sw}}\chi L_{\mathrm{w}}^{\mathrm{v}}}+\rho_{\mathrm{a}}\left(\frac{L_{\mathrm{w}}^{\mathrm{v}}M_{\mathrm{w}}}{R^{*}T}-1\right)}\right]^{2}\cdot\right.$$

$$\left.\cdot\left[1+\frac{1-2\frac{L_{\mathrm{w}}^{\mathrm{v}}M_{\mathrm{w}}}{R^{*}T}}{\left(\frac{L_{\mathrm{w}}^{\mathrm{v}}M_{\mathrm{w}}}{R^{*}T}-1\right)^{2}}\right]\right\}\cdot$$

$$\cdot N_{0\mathrm{R}}\cdot\left\{\frac{0.78\Gamma(2)}{\lambda_{\mathrm{R}}^{2}}+0.31Sc^{1/3}\left(\frac{k_{\mathrm{R}}\rho_{\mathrm{a}}}{\mu_{\mathrm{dif}}}\right)^{1/2}\left(\frac{p_{0}}{p}\right)^{0.2}\frac{\Gamma\left(\frac{n_{\mathrm{R}}}{2}+\frac{5}{2}\right)}{\lambda_{\mathrm{R}}^{\frac{n_{\mathrm{R}}}{2}+\frac{5}{2}}}\right\},$$

where Γ is the gamma-function.

The evaporation rate of melting solid hydrometeors (SMEV)

$$\text{(A.2)}\quad \mathrm{SMEV}=\frac{2\pi\left(\frac{q_{\mathrm{v}}}{q_{\mathrm{sw}}}-1\right)}{\frac{1}{q_{\mathrm{sw}}\chi}+\frac{L_{\mathrm{w}}^{\mathrm{v}}\rho_{\mathrm{a}}}{K_{\mathrm{a}}T}\left(\frac{L_{\mathrm{w}}^{\mathrm{v}}M_{\mathrm{w}}}{R^{*}T}-1\right)}\cdot$$

$$\cdot\left\{1-\frac{1}{2}\left(\frac{q_{\mathrm{v}}}{q_{\mathrm{sw}}}-1\right)\left[\frac{\rho_{\mathrm{a}}\left(\frac{L_{\mathrm{w}}^{\mathrm{v}}M_{\mathrm{w}}}{R^{*}T}-1\right)}{\frac{K_{\mathrm{a}}T}{q_{\mathrm{sw}}\chi L_{\mathrm{w}}^{\mathrm{v}}}+\rho_{\mathrm{a}}\left(\frac{L_{\mathrm{w}}^{\mathrm{v}}M_{\mathrm{w}}}{R^{*}T}-1\right)}\right]^{2}\cdot\right.$$

$$\left.\cdot\left[1+\frac{1-2\frac{L_{\mathrm{w}}^{\mathrm{v}}M_{\mathrm{w}}}{R^{*}T}}{\left(\frac{L_{\mathrm{w}}^{\mathrm{v}}M_{\mathrm{w}}}{R^{*}T}-1\right)^{2}}\right]\right\}\cdot$$

$$\cdot N_{0\mathrm{S}}\cdot\left\{\frac{0.78\Gamma(2)}{\lambda_{\mathrm{S}}^{2}}+0.31Sc^{1/3}\left(\frac{k_{\mathrm{S}}\rho_{\mathrm{a}}}{\mu_{\mathrm{dif}}}\right)^{1/2}\left(\frac{p_{0}}{p}\right)^{0.2}\frac{\Gamma\left(\frac{n_{\mathrm{S}}}{2}+\frac{5}{2}\right)}{\lambda_{\mathrm{S}}^{\frac{n_{\mathrm{S}}}{2}+\frac{5}{2}}}\right\}.$$

REFERENCES

[1] Kessler E., *Meteorol. Monograph*, **10** (1969) No. 32 (Boston: Am. Meteorol. Soc.).
[2] Lin Y.-L., Farley R. D. and Orvill H. D., *J. Clim. Appl. Meteorol.*, **22** (1983) 1065.
[3] Rutledge S. A. and Hobbs P. V., *J. Atmos. Sci.*, **40** (1983) 1200.
[4] Marecal V., Hauser D. and Roux F., *J. Atmos. Sci.*, **50** (1993) 975.
[5] Pressman D. JA., *Meteorologija i gidrologija (Meteorology and Hydrology)*, No. 11 (1994) 62, in Russian.
[6] Pressman D. JA., *Meteorologija i gidrologija (Meteorology and Hydrology)*, No. 6 (1996) 25, in Russian.
[7] Drofa O. V., *Meteorologija i gidrologija (Meteorology and Hydrology)*, No. 9 (1998) 41, in Russian.

[8] Schultz P., *Mon. Weather Rev.*, **123** (1995) 3331.
[9] *Oblaka i oblachnaja atmosfera (Clouds and cloudy atmosphere)*, Spravochnik pod red. (Handbook under redaction of) I. A. Mazina and A.KH. KHrgiana (L., Gidrometizdat) 1989, in Russian.
[10] Marshall J. S. and Palmer W., *J. Meteorol.*, **5** (1948) 165.
[11] Mason B. J., *The Physics of Clouds* (Oxford: Claredon Press) 1971, p. 671.
[12] Langleben M. P., *Q. J. R. Meteorol. Soc.*, **80** (1954) 174.
[13] Heymsfield A. J. and Kajikawa M., *J. Atmos. Sci.*, **7** (1987) 1088.
[14] Gunn R. and Kinzer G. D., *J. Meteorol.*, **6** (1949) 243.
[15] Foot G. P. and DuToit P. S., *J. Atmos. Sci.*, **8** (1969) 249.
[16] Fletcher N. H., *The Physics of Rainclouds* (Cambridge Univ. Press) 1962.
[17] Byers H. R., *Elements of Cloud Physics* (University of Chicago Press) 1965, p. 191.
[18] Srivastava P. C. and Coen J. L., *J. Atmos. Sci.*, **49** (1992) 1643.
[19] Beard K. V. and Pruppacher H. R., *J. Atmos. Sci.*, **28** (1971) 1455.
[20] Ogura Y. and Phillips N. A., *J. Atmos. Sci.*, **19** (1962) 173.
[21] Emde K., *Comparison of model simulation with observation of the CCOPE 19-th July 1981 case study, Report of the II International Cloud Modeling Workshop, Toulouse 8-12 August 1988.* WMP Report No. 11, WMO/TD No. 268, Geneva (1988).
[22] Kubesh R. J., Musil D. J., Farley R. D. and Orville H. D., *J. Appl. Meteorol.*, **27** (1988) 216.
[23] Farley R. D., *Simulation of the 2 August 1981 CCOPE hail-storm, Proceedings of the I International Cloud Modeling Workshop/Conf., WMO, Irsee, FRG, July, 1985*, pp. 99-110.
[24] Proctor F. H. and Bowles R. L., *Meteorol. Atmos. Phys.*, **49** (1992) 107.
[25] Lee W.-C. and Carbone R. E., *Mon. Weather Rev.*, **120** (1992) 2188.
[26] Mahoney III W. P. and Elmore K. L., *Mon. Weather Rev.*, **119** (1991) 176.
[27] Kingsmill D. E. and Wakimoto R. M., *Mon. Weather Rev.*, **119** (1991) 262.
[28] Miller L. J. and Fankhauser J. C., *J. Atmos. Sci.*, **40** (1983) 2399.
[29] Farley R. D., *J. Climate Appl. Meteorol.*, **26** (1987) 789.
[30] Pavlov N. F., *Aerologiya, radiometeorologiya i tehnika bezopastnosti (Aerology, radiometeorology and safety engineering)* (L., Gidrometizdat) 1980, in Russian.
[31] Doviak R. and Zrnich D., *Doplerovskie radiolokatoryi i meteorologicheskie nablyudeniya (Doppler radars and meteorological observations)* (L., Gidrometizdat) 1988, in Russian.
[32] Buzzi A., Fantini M., Malguzzi P. and Nerozzi F., *Meteorol. Atmos. Phys.*, **53** (1994) 137.
[33] Malguzzi P. and Tartaglione N., *Q. J. R. Meteorol. Soc.*, **125** (1999) 2291.
[34] Gyakum J. R., Carrera M., Zhang D.-L., Miller S., Caveen J., Benoit R., Black T., Buzzi A., Chouinard C., Fantini M., Folloni C., Katzfei J. J., Kuo Y.-H., Lalaurette F., Low-Nam S., Mailhot J., Malguzzi P., McGregor J. M., Nakamura M., Tripoli G. and Wilson C., *Weather and Forecasting*, **11** (1996) 521.
[35] Georgelin M., Bougeault P., T., Brzovic N., Buzzi A., Calvo J., Cassé V., Desgagné M., El-Khatib R., Geleyn J. F., Holt T., Hong S.-Y., Kato T., Katzefey J., Kurihara K., Lacroix B., Lalaurette F., Lemaitre Y., Mailhot J., Majewski D., Malguzzi P., Masson V., McGregor J., Minguzzi E., Paccagnella T. and Wilson C., *Q. J. R. Meteorol. Soc.*, **126** (2000) 991.
[36] Kain J. S. and Fritsch J. M., *J. Atmos. Sci.*, **47** (1990) 2784.
[37] Buzzi A. and Foschini L., *Meteorol. Atmos. Phys.*, **72** (2000) 131.
[38] Buzzi A., Tartaglione N. and Malguzzi P., *Mon. Weather Rev.*, **126** (1998) 2369.